



2D simulation of a microfluidic biosensor for CRP detection into a rotating micro-channel

Mohamed Bahri^{1,4} · Imen Dermoul² · Marshet Getaye^{1,3} · Mounir Ben Ali⁴ · Errachid Abdelhamid⁵

© Springer Nature Switzerland AG 2019

Abstract

Previously, pumping systems using centrifugal force has been regarded as an attractive control method for fluid flow interior microchannel. In this work, we propose a novel design of a biosensor for complex reactive protein detection in two-dimensional rotating microchannel using the finite element method. We have first developed the physical modeling of the centrifugal force driven, and detailed velocity profile and expended the pressure distribution. Several crucial factors that influence the equilibrium binding time are discussed, including the bulk analyte concentration and the biosensor length. The obtained analytical results reveal that the binding reaction is largely enhanced with the increase of the angular velocity. Hence, an appropriate choice of the angular velocity may enhance the microfluidic biosensor performance and reduce considerably the time response. This work can open new opportunity for further investigation in microflow injection experimental studies.

Keywords Biosensors · Microfluidics · Binding kinetics · Rotating microchannel · Finite element method · Modelling · Complex reactive protein (CRP)

1 Introduction

Over the past decades, the application of microfluidics [1] in the field of nanotechnology has become an active research field, which raises interesting points in miniaturized analytical systems application dedicated for biology and chemistry like the micro total analysis systems [2], the genomic and the proteomic analyses [3]. These kinds of analyses offered a ubiquitous treatment of patients with the advantages of minimizing reagents and sample volumes [4]. From a more fundamental point of view, the reduction of dimensions leads to the predominance of the surface effect, which has several advantages like the rise of the thermal transfers [5] and the trapping of molecules of interest [6]. Those advantages has brought a special

emphasis on the development of immunoassays for various biosensors applications [7]. In general, most of the immunoassay systems implicate the same kinetics of the specific binding of analytes and immobilized ligands, in which the concentration of the binding complex analytes-ligands on the reaction surface plays a key role [8]. Several techniques have been employed to quantify and detect such an analyte–ligand interactions. The most common techniques are electrochemical [9], fluorescence [10] and surface plasmon resonance [11].

Nowadays, there exists a great deal of research interest on how to monitor the patient which gets a high-risk epidemic like cardiovascular disease. The CRP present in human serum can be used as a clinical indicator of many inflammatory factors [12] when its value is going up to

✉ Mohamed Bahri, bahrimohamed@cigit.ac.cn | ¹University of Chinese Academy of Sciences, Beijing 100049, China. ²Preparatory Institute for Engineering of Nabeul IPEIN, University of Carthage, Campus Universitaire, Merazka, Nabeul, Tunisia. ³CAS Center of Excellence in Nanoscience, CAS Key Laboratory of Nanosystem and Hierarchical Fabrication, National Center for Nanoscience and Technology, Beijing 100190, China. ⁴Higher Institute of Applied Sciences and Technology of Sousse, GREENS ISSAT, University of Sousse, Ibn Khaldoun, 4003 Sousse, Tunisia. ⁵Institute of Analytic Sciences, UMR 5280, CNRS, Lyon 1 University, University of Lyon, ENS Lyon - 5, Rue de la Doua, 69100 Villeurbanne, France.



hundreds or even tens of times than the normal value (less than 1 µg/ml in a non-inflammatory human serum) [13]. Currently, many scientific researchers are developing various strategies to enhance the mass transport in microfluidic systems and improve the achievement of the target antigen to the sensitive surface. For example, Selmi et al. [14] developed a two-dimensional microfluidic confinement device for CRP detection, where the confinement flow velocity grew to enhance the binding rate. Also, Hofmann et al. [8] suggested a three dimensional microfluidic for immunoassays on a planar waveguide application, where a sample flow was joined with the perpendicular flow of a sample medium. Therefore, the increase in the makeup flow served to decrease the sample into a thin layer near the sensing surface. In an other study, Munir et al. [15] used the magnetic field force to improve the achievement of the tagging analyte with magnetic nanoparticles towards the sensing zone. Sigurdson et al. [16] developed a technique to enhance the response of microfluidic immuno-sensors by using the electro-kinetically-driven AC in order to improve the achievement of the antigen to the surface of the immobilized ligands. The binding rate can be raised by utilizing V root-mean square applied potential. Hart et al. [17] performed the heterogeneous immunoassays by applying an AC electro-osmosis through the use of the fluorescent immunoassays. Huang et al. [18] employed the finite element method to investigate the binding reaction of Immunoglobulin G (IgG) and CRP. Accordingly, a non-uniform AC electric field was applied to the flow microchannel of the biosensor to stir the flow. Importantly, the applied AC electric field reduced the thickness of the diffusion layer and accelerated the association and dissociation process. Hu et al. [19] used the electro-kinetic control technique to develop a new microfluidic chip based on polydimethylsiloxane, which was applied to heterogeneous immunoassays systems.

The development of highly advanced microfluidic systems, that generally include several microfluidic functions [2, 20] such as valve, pump, separation, mixing and reaction and so on, has become a major requirement to offer a lot of advantages such as real-time detection [2], high sensitivity and especially the ability to control the fluid flow in a precise manner. Among many controlling processes reported in the literature, the pressure driven flow and the electro-kinetics have been widely regarded as the most representative control methods of the fluid flow [21]. Electroosmotic flow has broadly been used for the analyses due to its appealing characteristic of a plug like a velocity profile [22]. Nevertheless, centrifugal flow schemes have been also deemed as a promising and an elegant means to carry fluids in microfluidic systems [23, 24]. This consists of micro-dimensional channel and reservoir which are fabricated on a disc similar to a compact disc. In addition,

the fluid drive is realised through the rotation of the disc platform. Such platform has already been used for biomedical diagnostic appliances [25]. This microfluidic CD system present numerous advantages including the easy operation, fast response, low cost and minimum sample usage, etc... [26]. Several microfluidic approaches toward sample detection and quantification such as protein assays [27] and cell lysis [28] have been widely studied.

Herein, we employed the finite element method to investigate the angular velocity effect on the pressure distribution and asses the improvement of the protein binding kinetics of a biosensor inside a rotating microchannel. We design the lab-on-a-chip platform using the Coriolis and the centrifugal forces to control the fluid flow. The two forces (Coriolis and centrifugal) were manipulated by changing the angular velocity of the disc. Such a platform is programmed by utilizing a controlled sequence of angular velocities. The centrifugal force provokes a parabolic flow outline in the radial direction similar to a Poiseuille or pressure driven flow. The velocity depends Coriolis force generates an inhomogeneous transverse force in the tangential meaning, which has its highest value in the middle of the channel. This work can open new opportunity for further investigation in microflow injection experimental studies.

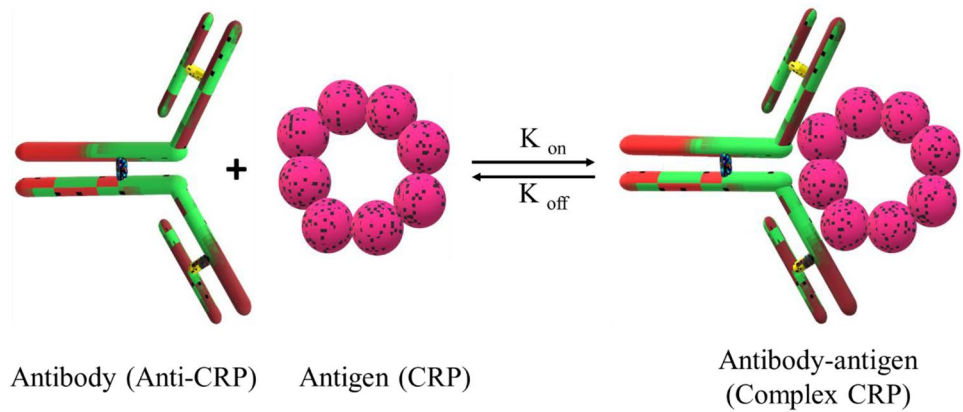
2 Theoretical model

The study was aimed at computing the kinetics of binding reaction between an analyte concentrations of CRP which is transported by a fluid toward a sensitive solid-liquid interface, where the ligands of antiCRP are immobilized. This interaction occurs at a 2D reaction surface of a biosensor with reaction kinetics where the analyte-ligand complex is formed. In our case, we suppose that our immunoassay system mixes a small concentration of biological analyte human CRP diluted in phosphate buffer solution as a neutral buffer solution which present physical properties similar to water [29]. The sum will be used as a carrier fluid. The binding reaction corresponding to the formation of the complex CRP is illustrated in Fig. 1 where K_{on} and K_{off} are the association and dissociation constant of CRP binding reaction, respectively.

2.1 Microchip design

In this paper, the analyte was manipulated utilizing the centrifugal and Coriolis forces to control the angular velocity variation of the disc, which is similar to the conventional compact disc players system or small bench scale centrifuges. The centrifugal force supplies an intrinsic means to carry the fluid from the inlet boundary through

Fig. 1 Schematic illustration of CRP binding reaction



an intended microfluidic processing structure to the outer boundary without a necessity for an external pumping. This whole phenomenon causes the development of a diffusion boundary layer depending on the ratio of the reaction rate (association or dissociation) and the flow velocity bordering the reaction surface. The investigated micro-channel is shown in Fig. 2.

In this particular work, the width and the length of the channel are 150 μm and 500 μm, respectively, with the assumption that the reaction surface has the same length with the biosensor, which is 40 μm in length and 3 μm in width. The center of the biosensor is located in the middle of the microchannel (250 μm at the X-axis), as shown in Fig. 2. The simulation was then carried using Navier–Stokes equations, Fick second law equation, and first-order Langmuir adsorption model.

2.2 The governing equations and problem set up

In this work, we develop an approach using the finite element method [30–32] for a microfluidic biosensor in a two-dimensional micro-channel with the calculation of the surface complex antibody-antigen formed versus time. A finite element software Comsol Multiphysics v5.2a (COMSOL, Sweden) [33] was used to organize a 2D simulation of momentum and mass transport in the microchannel and on the biosensor surface.

(1) Navier–Stokes equation

The fluid is incompressible into a centrifugal driven flow at an angular frequency $\omega = 2\pi\nu$ and governed via the Navier–Stokes equation [31, 34, 35] which can be given by:

$$\rho(\mathbf{u} \cdot \nabla)\mathbf{u} = -\nabla p + \eta \nabla^2 \mathbf{u} + \mathbf{F} \tag{1}$$

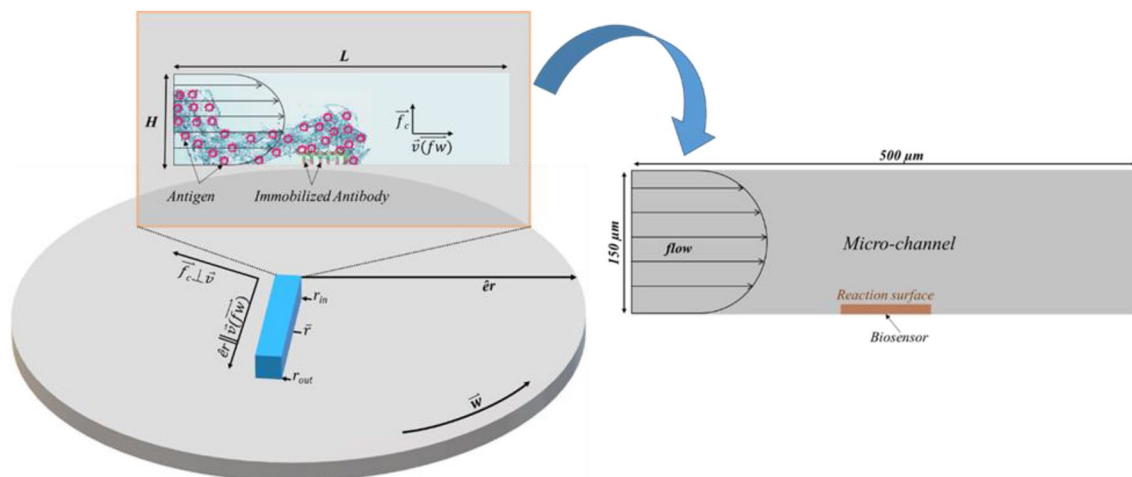


Fig. 2 Geometry and forces on a rotating disc at an angular velocity vector $\vec{\omega}$, the local radial unit vector is expressed by \hat{e}_r . The rectangular radial micro-channel exhibits a height H and a length L . The liquid plug is characterized by its inner and outer boundaries r_{in} and r_{out} respectively and a mean radial position \bar{r} . The centrifugal force f_w (Eq. 3) yield a parabolic profile \vec{v} mainly pointing in the

radial direction. The Coriolis force \vec{f}_c (Eq. 4) pursue to deflect the flow in the transversal direction. Due to the restriction of the transversal motion by the side walls, the flow field \vec{v} is non-uniform in the cross section of the channel and which leads to an inhomogeneous field distribution of the Coriolis force $\vec{f}_c \perp \vec{v}$

The continuity equation is

$$(\nabla \cdot \mathbf{u} = 0) \tag{2}$$

here \mathbf{u} is the velocity field, \mathbf{P} is the pressure, ρ and η are the density and the viscosity respectively. \mathbf{F} represent the total external force applied to the microchannel (the centrifugal and Coriolis forces).

The flow is transported in the radial direction ($\hat{\mathbf{e}}_r$) to drive the fluid into a parabolic velocity profile analogous to a pressure driven flow due to the centrifugal field ($\vec{\mathbf{f}}_w$) which is exerted on the fluid as the disc is spun [36] and is described by the following equation:

$$\vec{\mathbf{f}}_w = \rho r \vec{\omega}^2 \hat{\mathbf{e}}_r \tag{3}$$

where r is the radial position, $\hat{\mathbf{e}}_r$ is the radial direction and $\vec{\omega}$ is the angular frequency vector. The second force is perpendicular to the velocity profile and depends on the properties of the fluid is called the Coriolis force ($\vec{\mathbf{f}}_c$) [37] and it can be given by the following equation:

$$\vec{\mathbf{f}}_c = -2\rho r \vec{\omega} \vec{\mathbf{v}} \tag{4}$$

here $\vec{\mathbf{v}}$ is the velocity vector. The volume force conditions were applied by substituting the Eqs. (3) and (4) into Eq. (1), and these are used as \mathbf{X} and \mathbf{Y} -axis respectively.

(2) Fick second law equation

The analyte is transported to reach the sensitive layer, that could be described by the following equation [38]:

$$\frac{\partial[\mathbf{A}]}{\partial t} + \mathbf{u} \frac{\partial[\mathbf{A}]}{\partial x} + \mathbf{v} \frac{\partial[\mathbf{A}]}{\partial y} = \mathbf{D} \frac{\partial^2[\mathbf{A}]}{\partial x^2} + \frac{\partial^2[\mathbf{A}]}{\partial y^2} \tag{5}$$

where $[\mathbf{A}]$ is the bulk concentration of the analyte and \mathbf{D} is the diffusion coefficient of the analyte which is equal to $2.175 \times 10^{-11} \text{ m}^2/\text{s}$ for the human CRP, and \mathbf{u} and \mathbf{v} are the velocities in \mathbf{X} and \mathbf{Y} components respectively.

(3) First order Langmuir adsorption model equation

It is a chemical kinetics equation which is described using the first order Langmuir adsorption model [39, 40]. We assume that the analyte–ligand complex $[\mathbf{AB}]$ formed on the sensitive surface is immobilized without diffusion and is increased as a function of time according to the reaction rate equation as follows:

$$\frac{\partial[\mathbf{AB}]}{\partial t} = \mathbf{K}_{\text{on}}[\mathbf{A}]_{\text{surface}} \{[\mathbf{B}_0] - [\mathbf{AB}]\} - \mathbf{K}_{\text{off}}[\mathbf{AB}] \tag{6}$$

where $[\mathbf{A}]_{\text{surface}}$ is the concentration of the analyte at the reaction surface, $[\mathbf{B}_0]$ is the initial concentration of the

immobilized ligand. The CRP binding reaction parameters used to carry out the simulation are summarized on Table 1 [13]

2.3 Numerical method

The stationary simulation was performed in a rotating reference disk with non-slip boundary conditions at the walls and 0 Pa as a constant pressure boundary condition at the inlet and outlet of the microchannel. The flow is isotherm, laminar and steady. However, the fluid is initially assumed to be at rest and the initial conditions for the bulk analyte concentration $[\mathbf{A}]$ and the analyte–ligand complex concentration on the reaction surface $[\mathbf{AB}]$ were set zero. The dissociation phase of the CRP binding reaction is simulated by cutting the supply of the analyte at a time after the saturation of the binding reaction.

In this theoretical study, a micro-channel of length $\mathbf{L} = r_{\text{in}} - r_{\text{out}}$ was used which starts at the center of the disk (center of rotation) and a mean radial position $\bar{r} = \frac{1}{2}(r_{\text{in}} + r_{\text{out}})$ (see Fig. 2). For the fluid, we set the parameters of distilled water at room temperature ($\rho = 1000 \text{ kg m}^{-3}$, $\eta = 1 \text{ mPa s}$). Figure 2 shows the patterning of flow in a microfluidic channel rotating at an angular frequency $\vec{\omega}$ (counter clockwise rotation). The $\vec{\mathbf{f}}_w$ is the centrifugal force which generates a parabolic profile in the radial direction ($\hat{\mathbf{e}}_r$), and $\vec{\mathbf{f}}_c$ is the Coriolis force which pursues to swerve the flow in a transversal direction.

The solution of the previous equations using initial and boundary conditions in two dimensions have no numerical method and an analytical solution. Hence, the comsol simulation couples the transport of diluted species and laminar flow physics. An unstructured triangular mesh was used to discretize our domain. The region nearby the bio-sensor is more refined with finer triangular mesh quality for a better resolution [41], as shown in Fig. 3.

The time step was controlled by the numerical solver during the computations. Surface CRP complex concentration was performed using the first order derivative equation. To confirm that the numerical results are mesh independent and the convergence has been obtained, Fig. 4 shows the surface CRP complex concentration as a function of time for several mesh grids. In this case, we fix the concentration of CRP at 6.4 mol/m^3 . As can be clearly

Table 1 CRP binding constant

Parameters	Name	Value
\mathbf{K}_{on}	Association constant	$1 \times 10^4 \text{ m}^3/\text{mol s}$
\mathbf{K}_{off}	Dissociation constant	$2.6 \times 10^{-2} \text{ s}^{-1}$
\mathbf{B}_0	Immobilized ligand concentration	$1.4 \times 10^{-8} \text{ mol/m}^2$

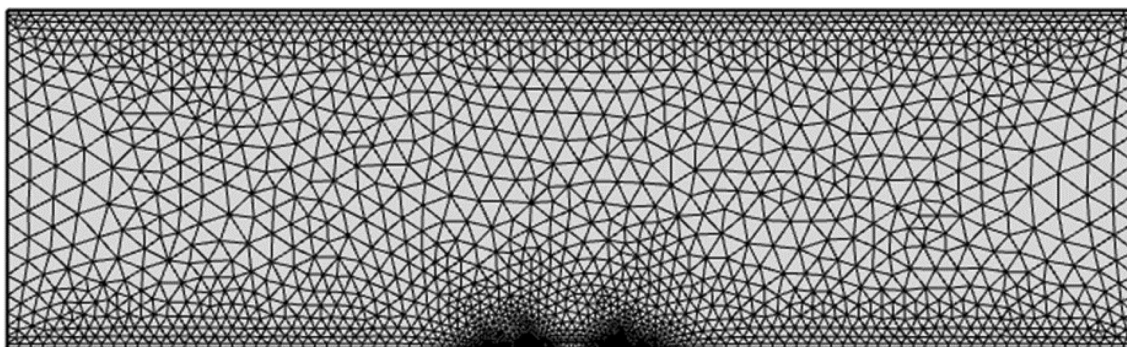


Fig. 3 The Two-dimensional unstructured geometry with triangular elements mesh

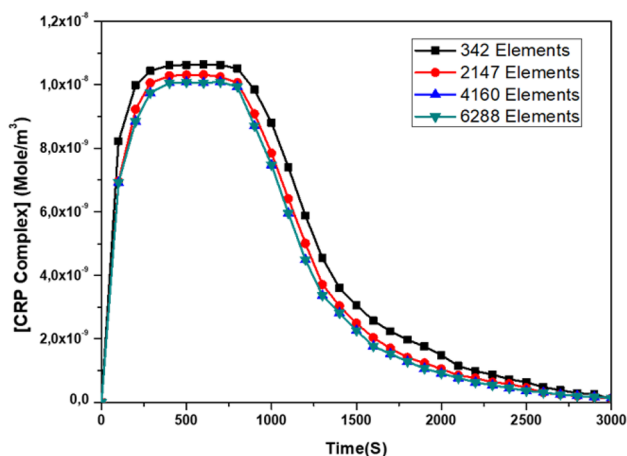


Fig. 4 Temporal evolution of [CRP complex] for several mesh grids

seen in Fig. 4, no significant difference was observed between the curves obtained using the three grids (2147, 4160, 6288 elements) so that the numerical convergence

has been reached [41, 42]. Unless specified, all simulations were done with a total elements number of 6288 elements.

3 Results and discussion

3.1 Binding kinetics of protein CRP

The temporal evolution of the surface complex concentration of the protein CRP versus different concentration of antigen analyte (64, 19.2, 6.4, 1.92, 0.64 and 0.192 mol/m³) is plotted and depicted in Fig. 5a. As expected, the rise in the bulk analyte concentration results in a growth of the biomolecule target quantities trapped on the sensitive surface. The numerical results are in a good agreement with the results reported by Yang et al. [13] and Selmi et al. [14], where there is a complex quantity formation on the sensitive surface as a function of analyte concentration.

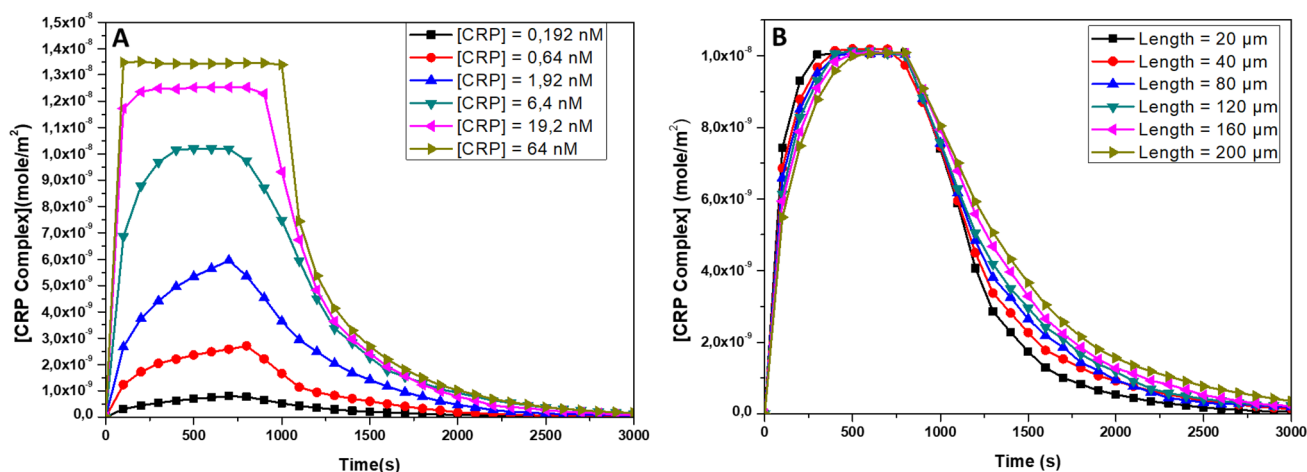


Fig. 5 The surface CRP complex concentration as a function of time for different bulk concentration of CRP (a) and different reaction surface length (b). The angular velocity is 100 rad/s

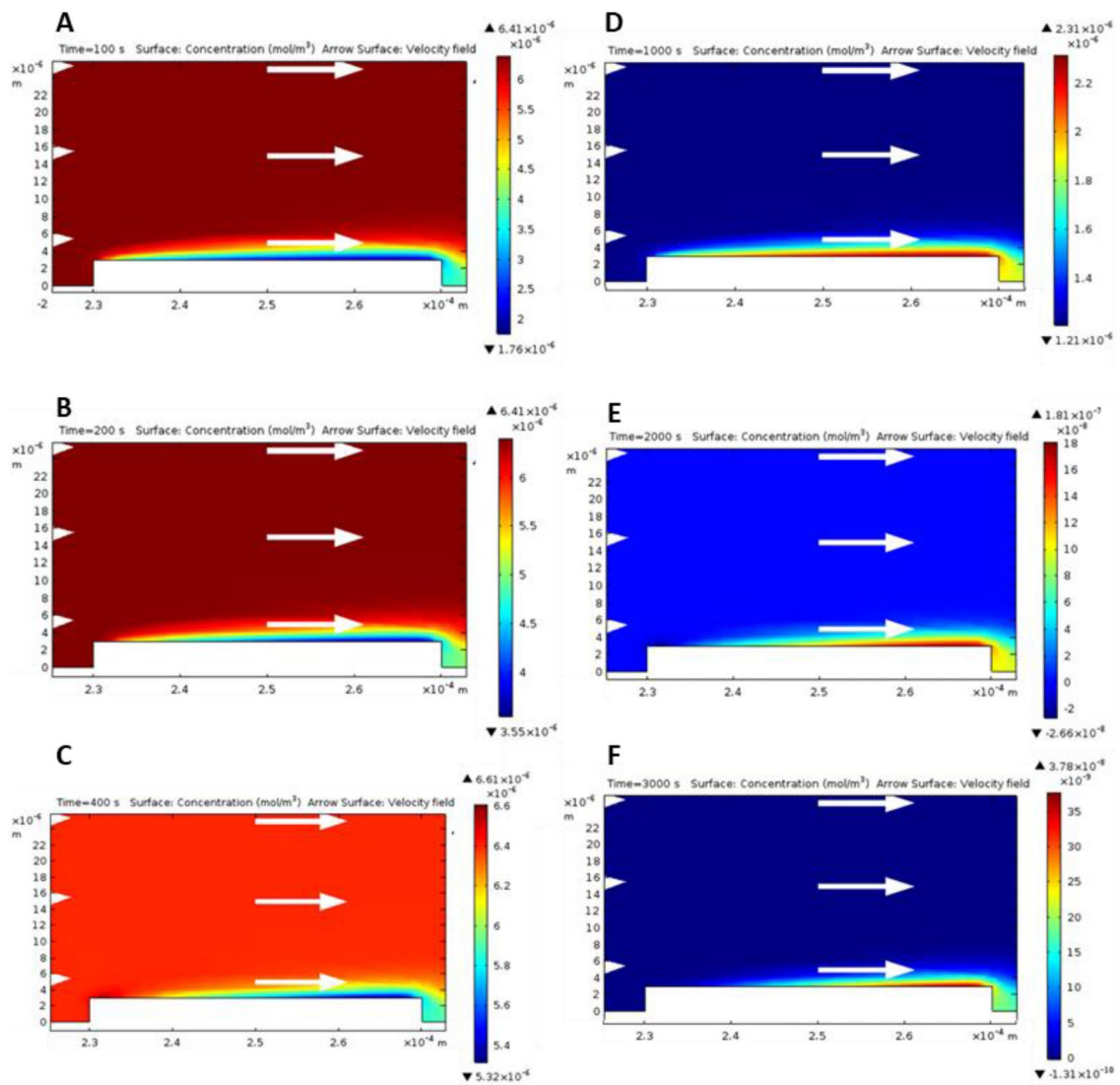


Fig. 6 The development of the diffusion boundary of the CRP binding reaction. The angular velocity is 100 rad/s and the bulk concentration is 6.4 mol/m³. The left three pictures (a–c) are in association

phase at times of 100, 200 and 400 s respectively and the right three pictures (d–f) are in dissociation phase at time of 1000, 2000, 3000 s respectively

3.2 Effect of the reaction surface length on the binding reaction kinetics

In order to study the effect of the reaction surface, we varied the length of microchannel from 20 to 200 μm. The concentration of the analyte and the angular velocity (w) was set to 6.4 mol/m³ and 100 rad/s, respectively, and the analyte was sustained at 1000 s. Figure 5b shows the temporal evolution of the CRP complex concentration as a function of a different length of the reaction surface. From Fig. 5b, it can be inferred that the time required to achieve the steady state condition gets longer when the boundary layer of the reaction surface is longer. While

minimizing the length of the reaction surface may be an obstruction due to the requirement of a sufficiently long reaction surface by some detecting technique. Thus, some compensation should be taken in consideration in the bio-sensor length design.

3.3 The development of the diffusion boundary layer

The CRP, as a large molecule of protein, is characterized by a low diffusion coefficient where it is limited by the mass transport coefficient [43] in a binding reaction of antibody-antigen structure. Also, it strongly depend on and limited by the diffusion coefficient and the flow velocity. Efficient

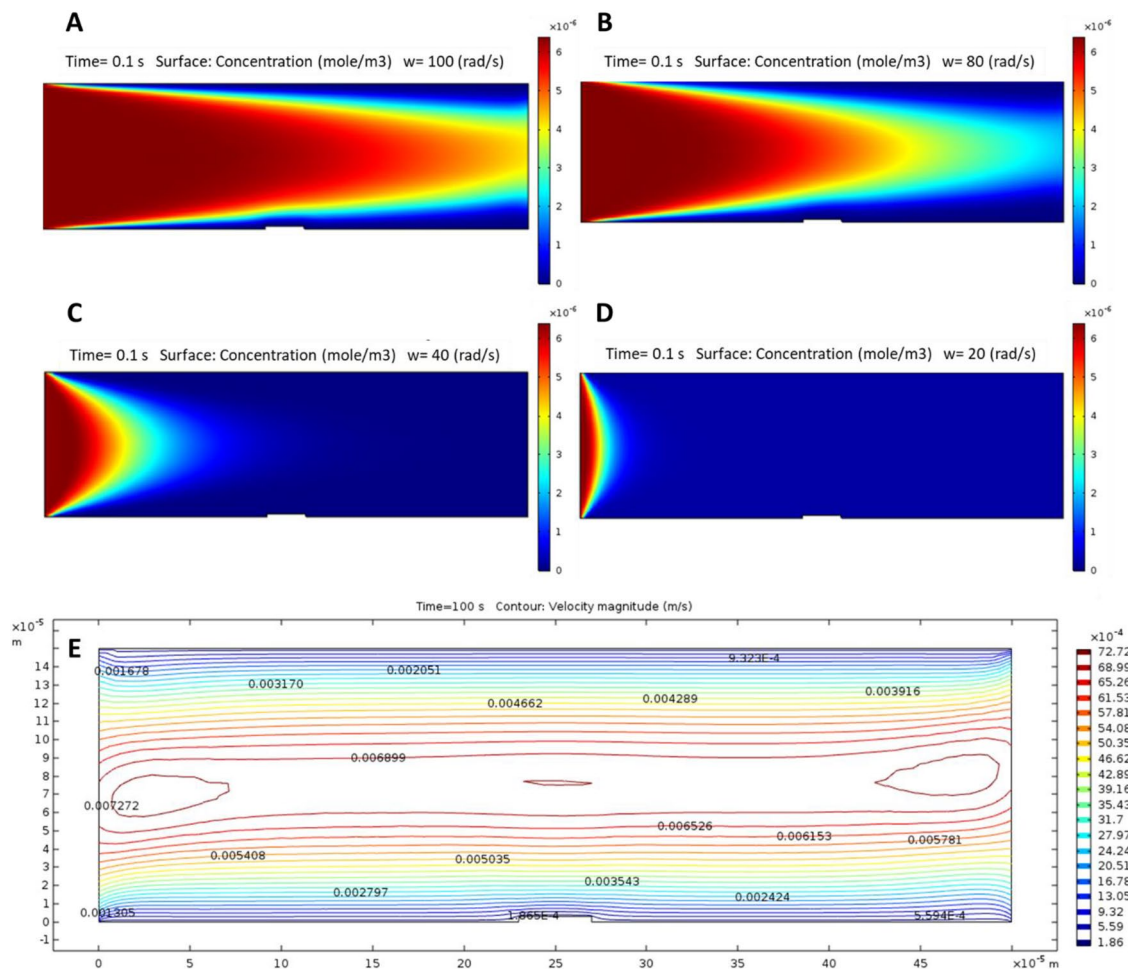


Fig. 7 The analyte and the velocity distribution inside the micro-channel after 0.1 s of simulation and with a constant analyte concentration $C = 6.4$ mol/m³. **a–d** The promotion of the analyte for different angular velocity corresponding to 100, 80, 40 and 20 rad/s

respectively. **e** The velocity distribution along the radial direction of the micro-channel, corresponding to an angular velocity of 100 rad/s

mass transport of fluid is characterized by a low diffusion boundary layer thickness [44]. Figure 6 shows the temporal evolution of the diffusion boundary layer of the CRP protein from the association phase (left panels; A, B, C) to the dissociation phase (right panels; D, E, F). For the sake of clarity, we have presented different density scales. Accordingly, the mass transport is along the reaction boundary in the same direction of the fluid. Furthermore, the uptake of $[A]_{\text{surface}}$ on the reaction surface is faster than the supply of the bulk in the association phase. Therefore, a small diffusion boundary layer of the analyte is constructed above the reaction surface. Hence, within the reaction surface boundary layer, there is a destitution of the analyte. In addition to the association phase, the diffusion boundary layer also occur in the dissociation phase when there is no

flow of analyte in system, and relatively denser concentration of the analyte can be seen on the boundary layer compared to that of the bulk [13].

3.4 Angular velocity effect on the binding reaction

The fluid flow is depends on the channel dimensions, the physical properties of the fluid and the angular frequency of the rolling platform. Therefore, raising angular velocity is an effective means to improve the mass transport and decrease the thickness of the diffusion boundary layer, as illustrated in Fig. 7a–d which are corresponding to 100, 80, 40, 20 rad/s respectively after 0.1 s of simulation. The centrifugal force generates a parabolic profile in the radial direction and play the role of pumping the system [45],

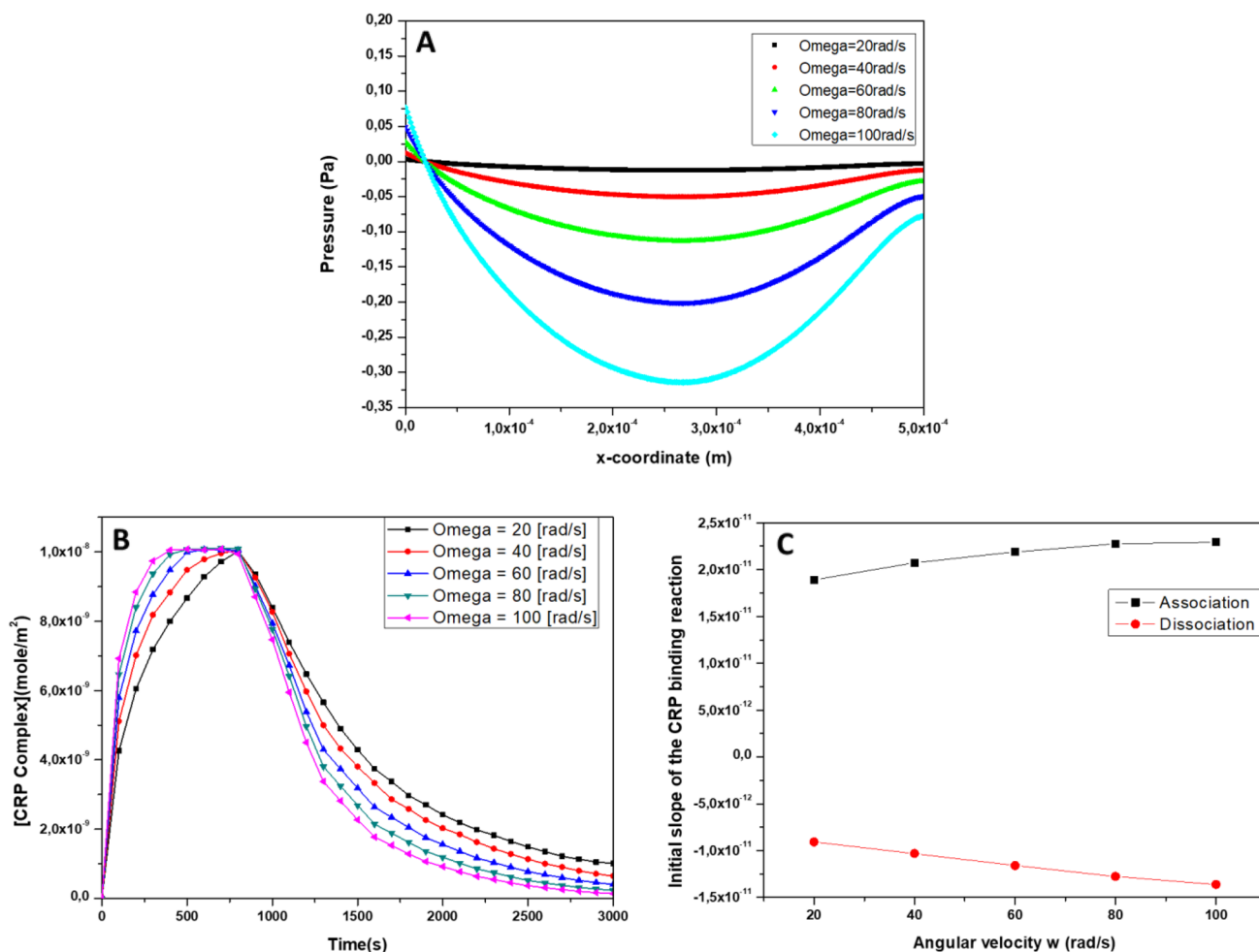


Fig. 8 Angular velocity effect on the pressure distribution and the CRP binding reaction for a CRP bulk concentration of 6.4 mol/m³. **a** The pressure distribution along the channel center from the inlet (0 μm) to the outlet (500 μm) for different angular velocity. **b** Tem-

poral evolution of the CRP surface complex concentration for various angular velocity 20, 40, 60, 80, 100 rad/s respectively. **c** The initial slope of CRP binding reaction as a function of angular velocity

which leads to the transportation of the fluid on a poiseuille flow profile in order to reach the reaction surface [37]. The velocity field depends on Coriolis force which normally produce an inhomogeneous transverse force and peaks in the center of the microchannel where the analyte is pushed toward the outlet boundary [37]. From there, the fluid escapes along up and down side walls due to the non slip boundary condition applied (Fig. 7e).

An appropriate measure of the pressure variation in the center of the microchannel as a function of the radial position was made to assess the simulation. Contrary to the pressure driven flow, the pressure fall along the rotation micro-channel is not linear which could be explained by the increase in the centrifugal force further away from the centre of rotation. The convex pressure profile for different angular velocity values (100, 80, 60 40, 20 rad/s) is displayed in Fig. 8a. Interestingly, the obtained numerical

results are in a good agreement with the one reported by Glatzel et al. [45] and Kim et al. [36], where a parabolic shape with negative value of pressure, along the micro-channel was obtained [36]. As a response to the rise of the centrifugal force along the radial direction, the pressure is expanded to maintain the same shear force all over the microchannel. A negative pressure slope in the left half region (the first 250 μm) is favorable to a small centrifugal force. Whereas, a positive pressure slope is in adverse to the flow to compensate the wide centrifugal in the right half region (the second 250 μm). These trends can be clarified by the force balance between the centrifugal force and the pressure gradient which match exactly with the average centrifugal force with zero pressure slope at the centre of the microchannel [45]. This is why a negative pressure distribution and a parabolic form is built along the microchannel. The increase in the angular velocity

from 20 to 100 rad/s leads to an enhancement of the pressure value in the centre of the microchannel which is multiplied 23 times going from -0.0132 to -0.312 Pa. As expected raising the angular velocity (w) is an effective means to reduce the thickness of the diffusion boundary layer. Figure 8b presents the effect of raising the angular velocity on the CRP binding kinetics. Therefore, the faster disc rotation is, the faster association and dissociation rates are.

Figure 8c shows the initial slope of the CRP binding reaction curves as a function of different angular velocity. Larger slopes were founded for higher angular velocity. This can be explained as faster diffusion in transporting the fluid for the micro-channel with higher angular velocity [46]. Increasing the angular velocity from 20 to 100 rad/s improve the initial slope from 1.89×10^{-11} to 2.29×10^{-11} and from -9.09×10^{-11} to -1.36×10^{-11} for the association and dissociation phases, respectively.

In this study, we have successfully made a new platform to conduct the fluid interior a rectangular microchannel with an efficient in term of time response and without the necessity for an external pumping system. Compared to the inlet flow velocity [13] as a conduction system, we get an improvement concerning the initial slope of the association phase of binding reaction from 1.8×10^{-11} to 2.29×10^{-11} . Recently, many attempts were made to improve such microfluidic transport system by superimposing another enhancement structure, namely, the use of the electrothermal force effect [38], the use of an obstacle above the biosensor [47], the confinement flow effect [14] and mixing electrothermal and confinement effect together [48].

4 Conclusion

In summary, the Coriolis and centrifugal forces are identified to be an efficient means to transport the fluid to the reaction surface of the biosensor and reduce significantly the time response. Several crucial factors such as the analyte concentration, the angular velocity and the length of the biosensor have been investigated theoretically. It is found that raising the angular velocity can effectively minimize the thickness of the diffusion boundary layer, and increase the fluid velocity. Hence, the association and dissociation rate of the protein binding reaction is drastically improved. In light of this, further investigation can be carried to study electrothermal and confinement flow effects on this rotating microchannel using 3D to design the biosensor device. We believe that this work can open new opportunity of research for further experimental investigation in microflow injection system.

Acknowledgements We are grateful to Professor Deqiang Wang and Chake Tlili for making available their laboratory facilities to us.

Compliance with ethical standards

Conflict of interest The authors declare that they have no conflict of interest.

References

1. Polson NA, Hayes MA (2001) Microfluidics: controlling fluids in small places. *Anal Chem* 73:312A–319A
2. Auroux P-A, Iossifidis D, Reyes DR, Manz A (2002) Micro total analysis systems. 2. Analytical standard operations and applications. *Anal Chem*. <https://doi.org/10.1021/ac020239t>
3. Sanders GH, Manz A (2000) Chip-based microsystems for genomic and proteomic analysis. *TrAC Trends Anal Chem* 19:364–378. [https://doi.org/10.1016/S0165-9936\(00\)00011-X](https://doi.org/10.1016/S0165-9936(00)00011-X)
4. Vyawahare S, Griffiths AD, Merten CA (2010) Miniaturization and parallelization of biological and chemical assays in microfluidic devices. *Chem Biol* 17:1052–1065. <https://doi.org/10.1016/J.CHEMBIOL.2010.09.007>
5. Das SK, Choi SUS, Patel HE (2006) Heat transfer in nanofluids—a review. *Heat Transf Eng* 27:3–19. <https://doi.org/10.1080/01457630600904593>
6. Freedman KJ, Otto LM, Ivanov AP, Barik A, Oh S-H, Edel JB (2016) Nanopore sensing at ultra-low concentrations using single-molecule dielectrophoretic trapping. *Nat Commun* 7:10217. <https://doi.org/10.1038/ncomms10217>
7. Soleymani L, Li F (2017) Mechanistic challenges and advantages of biosensor miniaturization into the nanoscale. *ACS Sensors* 2:458–467. <https://doi.org/10.1021/acssensors.7b00069>
8. Hofmann O, Voirin G, Niedermann P, Manz A (2002) Three-dimensional microfluidic confinement for efficient sample delivery to biosensor surfaces. Application to immunoassays on planar optical waveguides. *Anal Chem* 74:5243–5250. <https://doi.org/10.1021/ac025777k>
9. Lisdat F, Schäfer D (2008) The use of electrochemical impedance spectroscopy for biosensing. *Anal Bioanal Chem* 391:1555–1567. <https://doi.org/10.1007/s00216-008-1970-7>
10. Wolf M, Juncker D, Michel B, Hunziker P, Delamarche E (2004) Simultaneous detection of C-reactive protein and other cardiac markers in human plasma using micromosaic immunoassays and self-regulating microfluidic networks. *Biosens Bioelectron* 19:1193–1202. <https://doi.org/10.1016/j.bios.2003.11.003>
11. Wang J, Munir A, Zhou HS (2009) Au NPs-aptamer conjugates as a powerful competitive reagent for ultrasensitive detection of small molecules by surface plasmon resonance spectroscopy. *Talanta* 79:72–76. <https://doi.org/10.1016/j.talanta.2009.03.003>
12. Francis TJ, Tillett WS (1930) Serological reactions in pneumonia with a no-protein somatic fraction of Pnuemococcus. *J Exp Med* 24:561–571
13. Yang CK, Chang JS, Chao SD, Wu KC (2008) Effects of diffusion boundary layer on reaction kinetics of immunoassay in a biosensor. *J Appl Phys*. <https://doi.org/10.1063/1.2909980>
14. Selmi M, Echouchene F, Gazzah MH, Belmabrouk H (2015) Flow confinement enhancement of heterogeneous immunoassays in microfluidics. *IEEE Sensors J*. <https://doi.org/10.1109/jсен.2015.2475610>
15. Munir A, Wang J, Li Z, Zhou HS (2010) Numerical analysis of a magnetic nanoparticle-enhanced microfluidic surface-based

- bioassay. *Microfluid Nanofluid* 8:641–652. <https://doi.org/10.1007/s10404-009-0497-3>
16. Sigurdson M, Wang D, Meinhart CD (2005) Electrothermal stirring for heterogeneous immunoassays. *Lab Chip* 5:1366. <https://doi.org/10.1039/b508224b>
 17. Hart R, Lec R, Moses Noh H (2010) Enhancement of heterogeneous immunoassays using AC electroosmosis. *Sensors Actuators B Chem* 147:366–375. <https://doi.org/10.1016/j.snb.2010.02.027>
 18. Huang K-R, Chang J-S, Chao SD, Wu K-C, Yang C-K, Lai C-Y, Chen S-H (2008) Simulation on binding efficiency of immunoassay for a biosensor with applying electrothermal effect. *J Appl Phys* 104:064702. <https://doi.org/10.1063/1.2981195>
 19. Hu G, Gao Y, Sherman PM, Li D (2005) A microfluidic chip for heterogeneous immunoassay using electrokinetical control. *Microfluid. Nanofluidics* 1:346–355. <https://doi.org/10.1007/s10404-005-0040-0>
 20. Kovacs GTA (n.d.) *Micromachined transducers sourcebook*. McGraw-Hill Science/Engineering/Math; 1 edition (February 1, 1998), ISBN-10: 0072907223
 21. Pennathur S (2008) Flow control in microfluidics: Are the workhorse flows adequate? *Lab Chip* 8:383. <https://doi.org/10.1039/b801448p>
 22. Effenhauser CS, Bruin GJM, Paulus A (1997) Integrated chip-based capillary electrophoresis. *Electrophoresis* 18:2203–2213. <https://doi.org/10.1002/elps.1150181211>
 23. Ekstrand G, Holmquist C, Örléfors AE, Hellman B, Larsson A, Andersson P (2000) Microfluidics in a rotating CD. In: *Micro total analysis systems*. Springer, Dordrecht, pp 311–314. https://doi.org/10.1007/978-94-017-2264-3_71
 24. Gustafsson M, Hirschberg D, Palmberg C, Jörnvall H, Bergman T (2004) Integrated sample preparation and MALDI mass spectrometry on a microfluidic compact disk. *Anal Chem* 76:345–350. <https://doi.org/10.1021/ac030194b>
 25. Madou MJ, Kellogg GJ (1998) A centrifuge-based microfluidic platform for diagnostics. In: Cohn GE (ed) *International Society for Optics and Photonics*, pp 80–93. <https://doi.org/10.1117/12.307314>
 26. Lee J, Koelling KW, Lai S, Koh G, Juang Y-J, Yu L, Madou MJ, Lu Y, Daunert S (2001) Design and fabrication of CD-like microfluidic platforms for diagnostics: polymer-based micro-fabrication. *Biomed Microdevices* 3:339–351. <https://doi.org/10.1023/A:1012469017354>
 27. Duffy DC, Gillis HL, Lin J, Sheppard NF, Kellogg GJ (1999) Microfabricated centrifugal microfluidic systems: characterization and multiple enzymatic assays. *Anal Chem*. <https://doi.org/10.1021/ac990682c>
 28. Kim J, Hee Jang S, Jia G, Zoval JV, Da Silva NA, Madou MJ (2004) Cell lysis on a microfluidic CD (compact disc). *Lab Chip* 4:516. <https://doi.org/10.1039/b401106f>
 29. Yi M, Zhang H, Qi S, Li Q (2016) Determination of C-reactive protein concentration in serum based on chemiluminescence analysis. In: *Proceedings of 2016 8th international conference on measuring technology and mechatronics automation, ICMTMA 2016*, pp 214–217. <https://doi.org/10.1109/icmtma.2016.61>
 30. Chen Z (2005) *Finite element methods and their applications*. Springer, Berlin
 31. Molina DE, Medina AS, Beyenal H, Ivory CF (2019) Design and finite element model of a microfluidic platform with removable electrodes for electrochemical analysis. *J Electrochem Soc* 166:B125–B132. <https://doi.org/10.1149/2.0891902jes>
 32. Kuzmin D, Hämäläinen J (n.d.) *Finite element methods for computational fluid dynamics: a practical guide*. SIAM-Society for Industrial and Applied Mathematics (December 18, 2014), ISBN-10: 1611973600
 33. COMSOL Multiphysics® (n.d.) Modeling software. <https://www.comsol.com/>. Accessed 19 July 2019
 34. Snowden ME, King PH, Covington JA, Macpherson JV, Unwin PR (2010) Fabrication of versatile channel flow cells for quantitative electroanalysis using prototyping. *Anal Chem* 82:3124–3131. <https://doi.org/10.1021/ac100345v>
 35. Bird RB, Stewart WE, Lightfoot EN (2007) *Transport phenomena. Patterned and optimized*. <https://www.wiley.com/en-gb/Transport+Phenomena,+Revised+2nd+Edition-p-9780470115398>. Accessed 19 July 2019
 36. Kim DS, Kwon TH (2006) Modeling, analysis and design of centrifugal force driven transient filling flow into rectangular microchannel. *Microsyst Technol* 12:822–838. <https://doi.org/10.1007/s00542-006-0166-3>
 37. Ducrée J, Haeberle S, Brenner T, Glatzel T, Zengerle R (2006) Patterning of flow and mixing in rotating radial microchannels. *Microfluid Nanofluid* 2:97–105. <https://doi.org/10.1007/s10404-005-0049-4>
 38. Huang KR, Chang JS (2013) Three dimensional simulation on binding efficiency of immunoassay for a biosensor with applying electrothermal effect. *Heat Mass Transf* 49:1647–1658. <https://doi.org/10.1007/s00231-013-1214-z>
 39. Sadana A, Vo-Dinh T (1997) Antibody-antigen binding kinetics a model for multivalency antibodies for large antigen systems. *Appl Biochem Biotechnol* 67:1–22. <https://doi.org/10.1007/BF02787837>
 40. Zimmermann M, Delamarche E, Wolf M, Hunziker P (2005) Modeling and optimization of high-sensitivity, low-volume microfluidic-based surface immunoassays. *Biomed Microdevices* 7:99–110. <https://doi.org/10.1007/s10544-005-1587-y>
 41. Aoun N, Echouchene F, Diallo AK, Launay J, Belmabrouk H (2016) Finite-element simulations of the pH-ElecFET microsenors. *IEEE Sensors J*. <https://doi.org/10.1109/JSEN.2016.2585506>
 42. Nama N, Barnkob R, Mao Z, Kähler CJ, Costanzo F, Huang TJ (2015) Numerical study of acoustophoretic motion of particles in a PDMS microchannel driven by surface acoustic waves. *Lab Chip* 15:2700–2709. <https://doi.org/10.1039/C5LC00231A>
 43. Chaiken I, Rosé S, Karlsson R (1992) Analysis of macromolecular interactions using immobilized ligands. *Anal Biochem* 201:197–210. [https://doi.org/10.1016/0003-2697\(92\)90329-6](https://doi.org/10.1016/0003-2697(92)90329-6)
 44. Levich V (1962) *Physicochemical hydrodynamics*. Prentice-Hall, Englewood Cliffs. <http://www.worldcat.org/title/physicochemical-hydrodynamics/oclc/1378432>. Accessed 20 Oct 2017
 45. Glatzel T, Litterst C, Cupelli C, Lindemann T, Moosmann C, Niekrawietz R, Streule W, Zengerle R, Koltay P (2008) Computational fluid dynamics (CFD) software tools for microfluidic applications—a case study. *Comput Fluids* 37:218–235. <https://doi.org/10.1016/j.compfluid.2007.07.014>
 46. Brenner T, Glatzel T, Zengerle R, Ducrée J (2005) Frequency-dependent transversal flow control in centrifugal microfluidics. *Lab Chip* 5:146–150. <https://doi.org/10.1039/b406699e>
 47. Selmi M, Echouchene F, Belmabrouk H (2016) Analysis of microfluidic biosensor efficiency using a cylindrical obstacle. *Sens Lett*. <https://doi.org/10.1166/sl.2016.3527>
 48. Selmi M, Gazzah MH, Belmabrouk H (2016) Numerical study of the electrothermal effect on the kinetic reaction of immunoassays for a microfluidic biosensor. Undefined. <https://www.semanticscholar.org/paper/Numerical-Study-of-the-Electrothermal-Effect-on-the-Selmi-Gazzah/ef0ff48006d599f07eabc3dff0e86d0371f79670>. Accessed 10 Feb 2019

Publisher's Note Springer Nature remains neutral with regard to jurisdictional claims in published maps and institutional affiliations.